

# 000 BRIDGE DRIVE: DIFFUSION BRIDGE POLICY 001 FOR CLOSED-LOOP TRAJECTORY PLANNING IN 002 AUTONOMOUS DRIVING 003 004

006 **Anonymous authors**

007 Paper under double-blind review

## 011 ABSTRACT

012 Diffusion-based planners have shown great promise for autonomous driving due  
013 to their ability to capture multi-modal driving behaviors. However, guiding these  
014 models effectively in reactive, closed-loop environments remains a significant  
015 challenge. Simple conditioning often fails to provide sufficient guidance in com-  
016 plex and dynamic driving scenarios. Recent work attempts to use typical expert  
017 driving behaviors (*i.e.*, anchors) to guide diffusion models but relies on a truncated  
018 schedule, which introduces theoretical inconsistencies and can compromise per-  
019 formance. To address this, we introduce *BridgeDrive*, a novel anchor-guided dif-  
020 fusion bridge policy for closed-loop trajectory planning. Our approach provides a  
021 principled diffusion framework that effectively translates anchors into fine-grained  
022 trajectory plans, appropriately responding to varying traffic conditions. Our plan-  
023 ner is compatible with efficient ODE solvers, a critical factor for real-time au-  
024 tonomous driving deployment. We achieve state-of-the-art performance on the  
025 Bench2Drive benchmark, improving the success rate by **7.72%** over prior arts.

## 027 1 INTRODUCTION

028 Closed-loop planning with reactive agents is a critical challenge in autonomous driving, which re-  
029 quires effective interaction with complex and dynamic traffic environments (Jia et al., 2024). Diffu-  
030 sion models have become a powerful paradigm for this task due to their ability to model complex,  
031 multi-modal distributions and incorporate flexible guidance (Liao et al., 2025; Zheng et al., 2025b;  
032 Yang et al., 2024; Xing et al., 2025). A key challenge, however, is to determine which sources of  
033 guidance information are most salient and how to integrate them effectively into these models to  
034 produce plans that are not only plausible but also safe and reactive in real-world driving conditions.

035 A promising source for guidance is to leverage typical human expert driving behaviors, often repre-  
036 sented as coarse *anchor* trajectories, as they provide a strong prior for safe and sensible maneuvers,  
037 constraining the vast solution space. Recently, DiffusionDrive (Liao et al., 2025) implements this  
038 strategy by training a denoiser on a truncated diffusion schedule, starting from a noisy version of the  
039 anchor rather than pure Gaussian noise. While achieving state-of-the-art empirical performance, this  
040 approach introduces a theoretical inconsistency: its denoising process does not match the forward  
041 diffusion process that it is trained on, which diverges from the core principle of diffusion models  
042 and can lead to unpredictable behaviors and compromised performance.

043 To address this, we introduce *BridgeDrive*, a principled diffusion framework that integrates anchor-  
044 based guidance for autonomous driving planning using a theoretically sound diffusion bridge for-  
045 mulation. Instead of heuristically truncating the diffusion process, we formally define the planning  
046 task as learning a diffusion process that *bridges* the gap from a given coarse anchor trajectory to a  
047 refined, context-aware final trajectory plan. This formulation ensures that the forward and denoising  
048 processes are perfectly symmetric, allowing our model to learn a direct and robust transformation  
049 from anchors to final trajectories. By adhering to the principles of diffusion, our method fully  
050 leverages the expressive power of anchors for guidance while maintaining diffusion models' ability  
051 to represent diverse human-like driving behaviors. Furthermore, our approach is compatible with  
052 efficient ODE-based samplers, enabling real-time performance crucial for on-road deployment. Em-  
053 pirically, we achieve **74.99%** success rate on the Bench2Drive closed-loop evaluation benchmark,  
outperforming previous state-of-the-art method by a significant **7.72%** margin.

054 

## 2 PRELIMINARIES

055 

### 2.1 AUTONOMOUS DRIVING PLANNING AND EVALUATION

058 The planning task in autonomous driving can be formulated as predicting future trajectories of  
 059 the ego-vehicle based on raw sensor inputs. Conventionally, there are two trajectory representations  
 060 (Renz et al., 2025): (1) **Temporal speed waypoints**  $x := x^{\text{temp}} \in \mathbb{R}^{N_{\text{point}} \times 2}$ , represent equal  
 061 temporal-spaced (e.g., every 0.25 seconds) future coordinates of ego-vehicle, which inherently con-  
 062 tain speed control information. (2) **Geometric path waypoints**  $x := (x^{\text{geo}}, v) \in \mathbb{R}^{N_{\text{point}} \times 2} \times \mathbb{R}$ ,  
 063 represent equal geometric-spaced (e.g., every 1 meter) future coordinate of ego-vehicle; for geomet-  
 064 ric path waypoints-based planning, the model needs to predict the speed  $v$  of ego-vehicle. In this  
 065 paper, we choose to use geometric path waypoints as our model output, which differs from Diffu-  
 066 sionDrive Liao et al. (2025) where temporal speed waypoints are used. This design choice is based  
 067 on prior works (Chitta et al., 2023; Zimmerlin et al., 2024) and our ablation study in Section 4.

068 Evaluation of autonomous driving can be broadly categorized into open-loop and closed-loop set-  
 069 tings. The closed-loop setting is more challenging and can better reflect a policy’s real-world plan-  
 070 ning capability, since the ego vehicle’s decisions affect its own future states and those of the sur-  
 071 rounding agents, creating a feedback loop that can amplify small prediction errors over time. To  
 072 minimize the sim-to-real gap, closed-loop evaluation requires high-fidelity simulators to capture  
 073 the interactions between the ego vehicle and its surrounding environment, which are typically both  
 074 computationally expensive and time-consuming. CARLA (Dosovitskiy et al., 2017) has emerged as  
 075 the most widely used platform, with a series of benchmarks building on top of it, such as CARLA  
 076 Leaderboard, Longest6 (Chitta et al., 2023), and Bench2Drive (Jia et al., 2024). Interestingly, existing  
 077 methods that achieve near-perfect results on open-loop datasets, such as NavSim (Dauner et al.,  
 078 2024) or nuScenes (Caesar et al., 2019), still struggle to achieve comparable performance under  
 079 closed-loop evaluation (Li et al., 2024b; Liao et al., 2025; Fu et al., 2025; Renz et al., 2025). This  
 080 discrepancy emphasizes the inherent difficulty of closed-loop planning and highlights the need for  
 081 more robust methods to handle the complexities of dynamic, interactive traffic environments.

082 

### 2.2 DIFFUSION MODELS

083 Diffusion models (Sohl-Dickstein et al., 2015; Ho et al., 2020; Song et al., 2021a;b; Karras et al.,  
 084 2022) generate data  $x_0 \sim p_d(x_0)$  from pure Gaussian noise  $x_T \sim p(x_T) := \mathcal{N}(x_T | 0, \sigma_{\text{max}}^2 I)$   
 085 by reverting a forward diffusion process. Mathematically, the forward diffusion process, which  
 086 gradually corrupts data into noise, can be defined by a linear SDE (Song et al., 2021b):

$$dx_t = f(t)x_t dt + g(t)dw_t, \quad x_0 \sim p_d, \quad (1)$$

087 where  $t \in [0, T]$  denotes the diffusion timestep,  $f : [0, T] \rightarrow \mathbb{R}$  is the linear drift coefficient,  
 088  $g : [0, T] \rightarrow \mathbb{R}_+$  is the diffusion coefficient function, and  $w_t \in \mathbb{R}^d$  is a standard Brownian motion.  
 089 It turns out that this linear SDE owns a Gaussian transition kernel  $q(x_t | x_0) = \mathcal{N}(x_t | \alpha_t x_0, \sigma_t^2 I)$ ,  
 090 where  $\alpha_t = \exp\left(\int_0^t f(s)ds\right)$  and  $\sigma_t^2 = \alpha_t^2 \int_0^t \frac{g(s)^2}{\alpha_s^2} ds$  are the noise schedules (Kingma et al.,  
 091 2021). The forward SDE defines a series of marginal densities  $\{q(x_t)\}_{t \in [0, T]}$  along the diffusion  
 092 path, where  $q(x_t) = \int q(x_t | x_0) p_d(x_0) dx_0$ . Since  $q(x_T) \approx p(x_T)$  for sufficiently large  $T$ , we can  
 093 generate data  $x_0 \sim p_d(x_0)$  by transforming a noise sample  $x_T \sim p(x_T)$  through a probability flow  
 094 ODE (PF-ODE) (Song et al., 2021b):

$$\frac{dx_t}{dt} = f(t)x_t - \frac{g(t)^2}{2} \nabla_{x_t} \log q(x_t), \quad (2)$$

095 which shares identical marginal densities  $\{q(x_t)\}_{t \in [0, T]}$  as the forward SDE. The score function  
 096  $\nabla_{x_t} \log q(x_t)$  in Eq. (2) can be approximated by  $\nabla_{x_t} \log q(x_t) \approx (\alpha_t x_\theta(x_t, t) - x_t) / \sigma_t^2$  (Vincent,  
 097 2011), where the denoiser  $x_\theta(x_t, t)$  is parameterized by a neural network and learned by minimizing  
 098 the mean squared denoising error (Karras et al., 2022):

$$\min_{\theta} \mathbb{E}_{p(t)p_d(x_0)q(x_t | x_0)} [w(t) \|x_\theta(x_t, t) - x_0\|^2]. \quad (3)$$

099 For conditional generation, the denoiser  $x_\theta(x_t, t, z)$  takes in an extra conditional variable  $z$ , which  
 100 corresponds to the conditional score function  $\nabla_{x_t} \log q(x_t | z) \approx (\alpha_t x_\theta(x_t, t, z) - x_t) / \sigma_t^2$ . Fur-  
 101 thermore, Ho & Salimans (2021) propose to linearly interpolate between  $\nabla_{x_t} \log q(x_t | z)$  and  
 102  $\nabla_{x_t} \log q(x_t)$  with a hyperparameter to adjust the guidance strength of the conditional information.

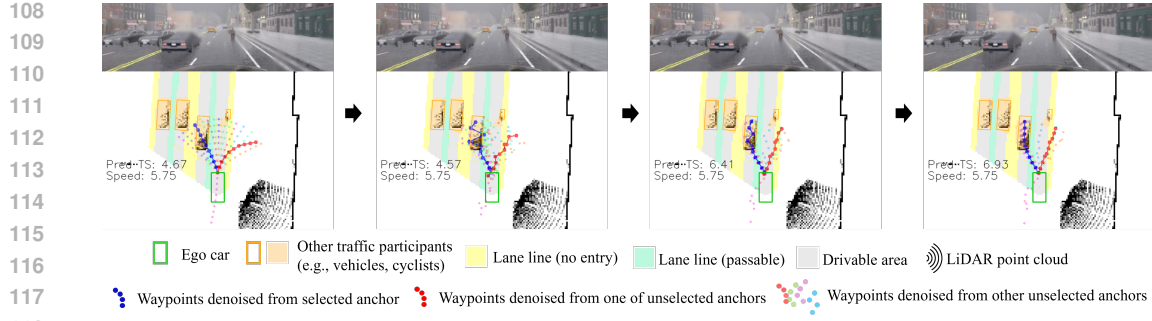


Figure 1: Visualization of the denoising process of BridgeDrive ( $t = T \rightarrow 0$  from left to right), with the leftmost figure being anchor  $x_T$  and the rightmost being the planned trajectory  $x_0$ . In each figure, the blue solid line depicts the denoised trajectory of the selected anchor at a specific timestep  $t$ , the red solid line depicts an example of the denoised trajectory of an un-selected anchor, and the rest scattered dots of other colors depict the denoised trajectories of other anchors at the timestep  $t$ . The red trajectory illustrates a failed case when a catastrophically wrong anchor is selected.

### 2.3 DIFFUSIONDRIVE WITH TRUNCATED DIFFUSION

DiffusionDrive (Liao et al., 2025) is a diffusion planner based on temporal speed waypoints, which leverages a truncated diffusion schedule and a fixed set of  $K$ -means clustered anchor trajectories  $\mathcal{Y} = \{y^i\}_{i=1}^{N_{\text{anchor}}}$  that represent typical human driving behaviors. The truncated forward diffusion process adds a small amount of noise to each anchor until  $t = T_{\text{trunc}} \ll T$  to obtain a set of noisy anchors  $\{y^i_{T_{\text{trunc}}}\}_{i=1}^{N_{\text{anchor}}}$ . The truncated denoising process starts from noisy anchors at  $t = T_{\text{trunc}}$ . Given conditional information  $z$  (e.g., sensor inputs and target point), a neural network  $x_{\theta}(\{y^i\}_{i=1}^{N_{\text{anchor}}}, t, z)$  is trained to predict the best anchor and output a denoised trajectory from the noisy version of the best anchor. The denoised trajectory is then used to compute the score function for denoising.

However, as discussed in the previous section, the learned denoising process of diffusion models must revert the forward diffusion process. Although DiffusionDrive demonstrates strong empirical performance, it utilizes a truncated diffusion schedule where the forward diffusion process adds noise to anchor trajectories and the denoising process attempts to recover the ground-truth trajectories. This design choice creates an asymmetry between its forward and denoising processes, framing the model’s task as regressing from noisy anchors to ground-truth trajectories, rather than as a reversal of the forward diffusion process.

## 3 BRIDGE DRIVE: DIFFUSION BRIDGE POLICY FOR TRAJECTORY PLANNING

To ensure the symmetry between the forward and backward processes of anchor-based diffusion planners, we propose a novel diffusion bridge policy, *BridgeDrive*, which provides a principled diffusion framework that leverages the powerful inductive biases of anchor-based guidance, while ensuring that the symmetry between the forward and denoising processes is maintained.

### 3.1 ANCHOR CONSTRUCTION FOR GEOMETRIC PATH WAYPOINTS

Anchors  $\mathcal{Y} = \{y^i\}_{i=1}^{N_{\text{anchor}}}$  are pre-defined, high-priority trajectories that represent typical human expert driving behaviors. They form a discrete set of atomic building blocks that planners use to construct solutions, which can dramatically reduce planning complexity, enforce safety constraints, improve robustness to dynamic environments, and align planning with task objectives (Chai et al., 2020; Chen et al., 2024; Li et al., 2024b). Our anchor definition is slightly different from Liao et al. (2025) since our model outputs geometric path waypoints as discussed in Section 2.1. Specifically, each anchor is formulated as<sup>1</sup>  $y := (x_y^{\text{geo}}, v_y) \in \mathbb{R}^{N_{\text{point}} \times 2} \times \mathbb{R}$ , where  $x_y^{\text{geo}} \in \mathbb{R}^{N_{\text{point}} \times 2}$  represents a series of coordinates of future path,  $N_{\text{point}}$  is the geometric prediction horizon, and  $v_y$  denotes the

<sup>1</sup>The subscript in  $x_y, v_y$  indicates that the trajectory and its speed *belongs to an anchor*, which differs from an ordinary trajectory  $x$  and its speed  $v$ . The superscript index  $i$  in  $y^i$  is omitted for notation simplicity.

162 anchor speed. Each anchor trajectory  $x_y^{\text{geo}}$  is defined as a  $K$ -means clustering center of the training  
 163 set, and the anchor speed  $v_y$  is defined as the average speed of the trajectories in the training set that  
 164 belong to this anchor. All values are normalized to the ego-vehicle coordinate system.  
 165

<b>Algorithm 1</b> BridgeDrive Training (ours)	<b>Algorithm 2</b> DiffusionDrive Training
1: Initialize $\theta$ # denoiser parameter	1: Initialize $\theta$ # denoiser parameter
2: <b>repeat</b>	2: <b>repeat</b>
3: $x, y, z \sim p_d(x, y, z)$	3: $x, y, z \sim p_d(x, y, z)$
4: # $x$ : GT traj, $y$ : anchor, $z$ : guidance	4: # $x$ : GT traj, $y$ : anchor, $z$ : guidance
5: $t \sim p(t)$ # $t \in [0, T]$	5: $t \sim p_{\text{trunc}}(t)$ # $t \in [0, T_{\text{trunc}}]$
6: $\epsilon \sim \mathcal{N}(0, I)$ # random noise	6: $\epsilon \sim \mathcal{N}(0, I)$ # random noise
7: $x_t = a_t y + b_t x + c_t \epsilon$ # noisy trajectory	7: $y_t = \alpha_t y + \sigma_t \epsilon$ # noisy anchor
8: Update $\theta$ with the gradient	8: Update $\theta$ with the gradient
	$w(t) \nabla_{\theta} \ x_{\theta}(x_t, t, y, z) - x\ ^2$
9: <b>until</b> convergence	9: <b>until</b> convergence
10: <b>return</b> $\theta$	10: <b>return</b> $\theta$

### 181 3.2 A GENERATIVE PARADIGM FOR ANCHOR-GUIDED DIFFUSION POLICY

183 To incorporate anchors into diffusion models in a principled way, we propose to factorize the joint  
 184 distribution of the ground-truth trajectory  $x$ , anchor  $y$ , and guidance information  $z$  as

$$185 \quad p_d(x, y, z) = p_d(x|y, z)p_d(y|z)p_d(z). \quad (4)$$

186 This factorization defines a two-step generative process. First, for a driving scene  $z \sim p_d(z)$ , we  
 187 sample an anchor  $y \sim p_d(y|z)$  given the scene information in  $z$  (e.g., BEV, agent/map queries, and  
 188 a target point). Then, the planned trajectory  $x \sim p_d(x|y, z)$  is generated according to the guidance  
 189 of the chosen anchor  $y$  and scene information  $z$ .  
 190

191 We propose to parameterize the conditional planning distribution  $p_d(x|y, z)$  with a conditional diffu-  
 192 sion bridge model  $p_{\theta}(x_t|x_T, z)$ , which constructs a diffusion bridge (Zhou et al., 2024; Zheng et al.,  
 193 2025a) between the ground-truth trajectory  $x_0 := x$  and anchor  $x_T := y$  (Doob & Doob, 1984):

$$194 \quad dx_t = f(t)x_t dt + g(t)^2 \nabla_{x_t} \log q(x_T|x_t) + g(t)dw_t, \quad x_0 \sim p_d, \quad x_T = y, \quad (5)$$

195 where  $t \in [0, T]$  denotes the diffusion timestep, the definitions of  $f(t), g(t)$  follow those in Eq. (1),  
 196 and  $\nabla_{x_t} \log q(x_T|x_t) = \nabla_{x_t} \log q(x_t|x_0, x_T) - \nabla_{x_t} \log q(x_t|x_0)$ . It turns out that Eq. (5) also owns  
 197 an analytical Gaussian transition kernel for any given trajectory  $x_0$  and anchor  $x_T$ :

$$198 \quad q(x_t|x_0, x_T) = \mathcal{N}(x_t|a_t x_T + b_t x_0, c_t^2 I), \quad (6)$$

$$199 \quad a_t = \alpha_t \gamma_t^2 / \alpha_T, \quad b_t = \alpha_t (1 - \gamma_t^2), \quad c_t^2 = \sigma_t^2 (1 - \gamma_t^2), \quad (7)$$

200 where  $\alpha_t = \exp\left(\int_0^t f(s)ds\right)$ ,  $\sigma_t^2 = \alpha_t^2 \int_0^t \frac{g(s)^2}{\alpha_s^2} ds$ , and  $\gamma_t = \frac{\alpha_T \sigma_t}{\alpha_t \sigma_T}$  (Zheng et al., 2025a), which  
 201 defines a diffusion bridge  $x_t = a_t x_T + b_t x_0 + c_t \epsilon_t$  that interpolates between  $x_0$  and  $x_T$  with  
 202 added Gaussian noise  $c_t \epsilon_t$ . Zhou et al. (2024) show that there exists a PF-ODE that shares identical  
 203 marginal densities  $\{q(x_t|x_T)\}_{t \in [0, T]}$  as the forward diffusion bridge SDE in Eq. (5):  
 204

$$205 \quad \frac{dx_t}{dt} = f(t)x_t - g(t)^2 \left( \frac{\nabla_{x_t} \log q(x_t|x_T, z)}{2} - \nabla_{x_t} \log q(x_T|x_t) \right), \quad (8)$$

206 which allows us to translate an anchor  $x_T$  to a planned trajectory  $x_0$  given the driving scene  $z$ .  
 207 To simulate this PF-ODE, we need to approximate the score function  $\nabla_{x_t} \log q(x_t|x_T, z)$  for the  
 208 conditional diffusion bridge model. In the next section, we will introduce our training and planning  
 209 algorithms for this diffusion bridge policy.  
 210

### 211 3.3 TRAINING AND PLANNING ALGORITHMS

212 In our diffusion bridge planner, each diffusion bridge is constructed between a ground-truth trajec-  
 213 tory  $x_0 := x$  and the nearest anchor  $x_T := y \in \mathcal{Y}$  to it. During training, we fit a neural network  
 214

216

**Algorithm 3** BridgeDrive Planning

217

218

219

220

221

222

223

224

225

226

227

228

229

230

231

---

```

1:  $z \sim p_d(z)$                                      # sample a driving scene
2:  $x_T = h_\phi(z, \mathcal{Y})$                          # choose which anchor to use
3: for  $i = N, \dots, 1$  do                      # discretize timesteps into  $T := t_N < \dots < t_1 < t_0 := 0$ 
4:    $\hat{x}_{0|t_i} = x_\theta(x_{t_i}, t_i, x_T, z)$       # compute the denoised mean trajectory
5:    $\hat{s}_{t_i} = (a_{t_i}x_T + b_{t_i}\hat{x}_{0|t_i} - x_{t_i})/c_{t_i}^2$   # compute the score function
6:    $d_{t_i} = f(t_i)x_{t_i} - g(t_i)^2(\hat{s}_{t_i}/2 - \nabla_{x_{t_i}} \log q(x_T|x_{t_i}))$   # compute the derivative  $dx_t/dt$ 
7:    $x_{t_{i-1}} = \text{ODESolverStep}(x_{t_i}, d_{t_i}, t_i, t_{i-1})$       # simulate the diffusion bridge PF-ODE
8: end for
9: return  $x_0$ 

```

---

denoiser  $x_\theta(x_t, t, x_T, z)$  to predict the denoising mean  $\hat{x}_{0|t} \approx \mathbb{E}[x_0|x_t, x_T, z]$  given noisy trajectory  $x_t \sim q(x_t|x_0, x_T)$  at timestep  $t$ , the nearest anchor  $x_T = y$  to  $x_0$ , and the conditional information  $z$  for the driving scene. This denoiser is trained by minimizing the mean squared denoising error:

$$\min_{\theta} \mathbb{E}_{p(t)p_d(x_0, x_T, z)q(x_t|x_0, x_T)} [w(t)\|x_\theta(x_t, t, x_T, z) - x_0\|^2]. \quad (9)$$

Our training algorithm is summarized in Algorithm 1. Notice that our forward and reverse diffusion paths both result in the end point  $x_0 = x$  since  $a_0 = c_0 = 0$  and  $b_0 = 1$ , ensuring that the denoiser is trained to reverse the forward diffusion process. On the other hand, in DiffusionDrive (Liao et al., 2025) (Algorithm 2), for all  $\alpha_t$  and  $\sigma_t$ , the noisy anchor  $y_t$  deviates from  $x$ , failing to adhere to the symmetry requirement of diffusion models. Also, the training procedure of BridgeDrive is simulation-free, which allows us to efficiently train the denoiser without simulating the forward SDE in Eq. (5) or the PF-ODE in Eq. (8). In addition, since the ground-truth trajectory  $x_0$  is not available for computing the nearest anchor  $y$  at inference time, we also train a classifier  $h_\phi(z, \mathcal{Y})$  to predict the nearest anchor  $y$  to  $x_0$  given  $z$  with the cross entropy loss.

Similar to standard diffusion models, the trained denoiser  $x_\theta(x_t, t, x_T, z)$  can be used to approximate the conditional score function for our conditional diffusion bridge model (Zheng et al., 2025a):

$$\nabla_{x_t} \log q(x_t|x_T, z) \approx \frac{a_t x_T + b_t x_\theta(x_t, t, x_T, z) - x_t}{c_t^2}. \quad (10)$$

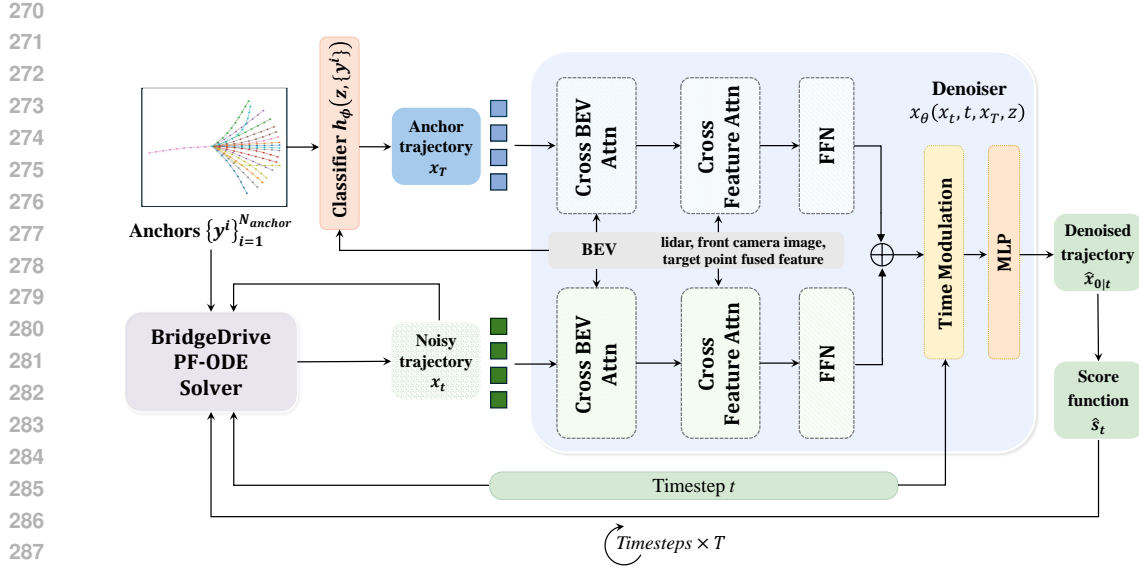
Our planning algorithm is summarized in Algorithm 3 and depicted in Fig. 2. Specifically, for a given driving scene  $z$ , we first use the classifier  $h_\phi(z, \mathcal{Y})$  to choose an anchor  $y \in \mathcal{Y}$ , which is the starting point  $x_T = y$  of the denoising process in our diffusion bridge planner. Then, we iteratively compute the denoised mean trajectory  $\hat{x}_{0|t}$  using our denoiser  $x_\theta(x_t, t, x_T, z)$ , calculate the score function  $\hat{s}_t$  using Eq. (10), and simulate the PF-ODE in Eq. (8) with the score  $\hat{s}_t$  using a numerical ODE solver. Although image diffusion models use higher-order ODE solvers (Karras et al., 2022; Lu et al., 2022) to accelerate sampling, we find that first-order methods, such as the DDIM sampler (Song et al., 2021a), are sufficient for the planning task with minimal number of function evaluations. Fig. 1 visualizes the denoising process of BridgeDrive for an example driving scenario.

## 3.4 MODEL ARCHITECTURE

Our model consists of three major components: perception module, denoiser, and classifier. Implementation and training details are provided in Appendix C.

**Perception Module.** The perception module extract useful features from lidar, front camera image, and target point for the downstream diffusion planner. We use a pre-trained perception backbone from TransFuser++ (Jaeger et al., 2023) to obtain BEV segmentation, bounding boxes of traffic participants, general traffic information (e.g., stop signs and traffic lights), and fused features from the inputs. The output of the perception module is denoted as  $z$  and will be used as the conditional guidance information in the denoiser module  $x_\theta(x_t, t, x_T, z)$ .

**Denoiser.** The architecture of the denoiser  $x_\theta(x_t, t, x_T, z)$  is illustrated in the light blue box in Fig. 2. For a noisy trajectory  $x_t$  at timestep  $t$  and its corresponding anchor  $x_T = y$ , we first interact them with BEV via deformable spatial cross-attention modules. Subsequently, cross-attention with fused features from lidar, front camera, and target point is applied. The resulting feature vectors



324  
 325 Table 1: Comparison between BridgeDrive and previous baselines on Bench2Drive. Our method  
 326 shows SOTA performance on both Driving Score (DS) and Success Rate (SR). Notably, by using a  
 327 principled diffusion bridge model, our method achieves significant improvements over previous dif-  
 328 fusion baselines (including those with prior knowledge from VLA), demonstrating the effectiveness  
 329 of the diffusion module in the autonomous driving task when following our paradigm as discussed  
 330 in Section 3.2. A potential avenue to further improve our method is to integrate prior knowledge  
 331 from VLA, which is left as future work.

Method	Expert	VLA	Diffusion	DS	SR(%)
DiffusionDrive <sup>temp</sup> (Liao et al., 2025)	PDM-Lite	✗	✓	77.68	52.72
DiffusionDrive <sup>geo</sup> (Liao et al., 2025)	PDM-Lite	✗	✓	80.79	58.18
TCP-traj* (Wu et al., 2022)	Think2Drive	✗	✗	59.90	30.00
UniAD-Base (Hu et al., 2023)	Think2Drive	✗	✗	45.81	16.36
VAD (Jiang et al., 2023)	Think2Drive	✗	✗	42.35	15.00
DriveTransformer (Jia et al., 2025)	Think2Drive	✗	✗	63.46	35.01
ORION (Fu et al., 2025)	Think2Drive	✓	✗	77.74	54.62
ORION diffusion (Fu et al., 2025)	Think2Drive	✓	✓	71.97	46.54
SimLingo (Renz et al., 2025)	PDM-Lite	✓	✗	85.07	67.27
TransFuser++ (Zimmerlin et al., 2024)	PDM-Lite	✗	✗	84.21	67.27
BridgeDrive (ours)	PDM-Lite	✗	✓	87.99 <sub>(+2.92)</sub>	74.99 <sub>(+7.72)</sub>

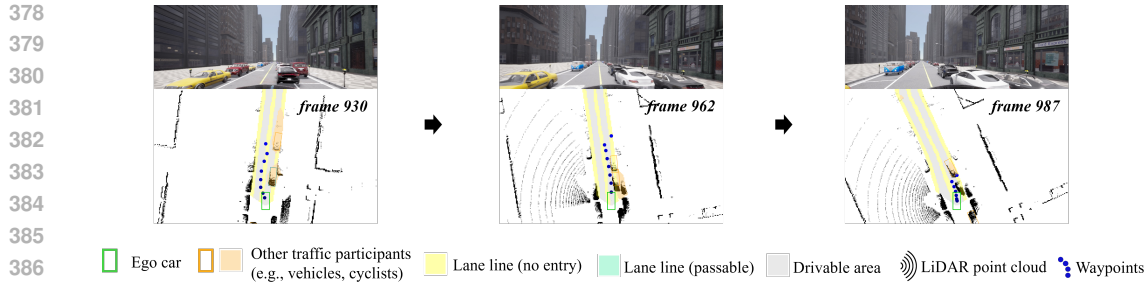
347  
 348 **Baselines.** We compare against the following baselines. *TCP-traj* (Wu et al., 2022) is a monocular  
 349 camera-based method that jointly learns planning and direct control with a situation-based fusion.  
 350 *UniAD* (Hu et al., 2023) is a unified end-to-end framework that integrates full-stack driving tasks  
 351 through query-based interfaces. *VAD* (Jiang et al., 2023) is an end-to-end vectorized paradigm that  
 352 models driving scenes with vectorized representations. *DriveTransformer* (Jia et al., 2025) employs  
 353 task parallelism, sparse representation, and streaming to enable efficient cross-task knowledge trans-  
 354 fer and temporal fusion. *ORION* (Fu et al., 2025) integrates a QT-Former for history aggregation,  
 355 a reasoning large language model (LLM), and a VAE for planning. *Simlingo* (Renz et al., 2025) leverages  
 356 VLA and achieves current SOTA performance on Bench2Drive. *TransFuser++* (Chitta  
 357 et al., 2023) (Zimmerlin et al., 2024) (Jaeger et al., 2023) ranks second in the 2024 CARLA chal-  
 358 lenge and first on the Bench2Drive test routes. In addition, we adapt *DiffusionDrive* to Bench2Drive  
 359 benchmark (denoted as *DiffusionDrive<sup>temp</sup>*). Adaptation details are provided in Appendix C.2.

## 4.2 MAIN RESULTS

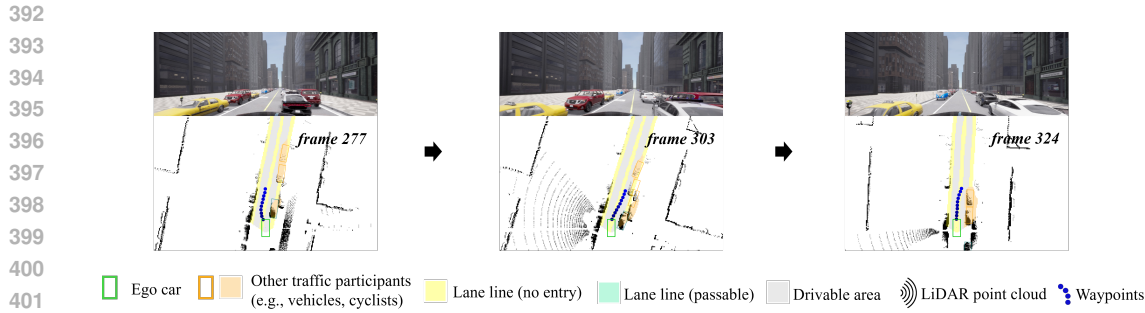
360 Evaluation results on Bench2Drive benchmark are demonstrated in Table 1. For all models that  
 361 exceeded previous SOTA result, we performed experiments with three random seeds to ensure re-  
 362 producibility. The performance of our work significantly exceeds that of all previous work. In  
 363 particular, our BridgeDrive outperform the SimLingo (Renz et al., 2025), the latest SOTA, by +1.8  
 364 and +5% in driving score and success rate, respectively. Moreover, BridgeDrive exhibits outstand-  
 365 ing multi-ability capability, especially in Merging (+10.87), and Traffic Sign (+7.02), resulting in over-  
 366 all improvement by +6.12 than SOTA, as shown in Table 4 in the Appendix. However, BridgeDrive  
 367 demonstrates suboptimal performance in the Comfortness and Give Way metrics, suggesting a ten-  
 368 dency toward frequent or poorly timed braking. This outcome may imply that our model prioritizes  
 369 safety considerations, potentially at the expense of passenger comfort. Furthermore, the inference  
 370 speed of BridgeDrive is suitable for real-time deployment, as detailed in Table 5. **Additional results**  
 371 **on the NAVSIM dataset are provided in Table 6.**

## 4.3 ABLATION STUDY AND QUALITATIVE ANALYSIS

372 The primer focus of this paper is on the design and study of diffusion models for trajectory planning;  
 373 therefore, we prioritize the most vital aspects that could influence the performance, namely 1) what  
 374 kind of trajectory representation is more compatible with diffusion model; 2) how our diffusion



388 Figure 3: A consecutive four frames of a sample Bench2Drive scene. Overtaking maneuver per-  
389 formed by **BridgeDrive<sup>temp</sup>**. The ego car exhibited deficiencies in overtaking maneuver coordi-  
390 nation and speed control, which directly led to a collision with the white vehicle. For video demon-  
391 stration, please refer to supplementary materials.

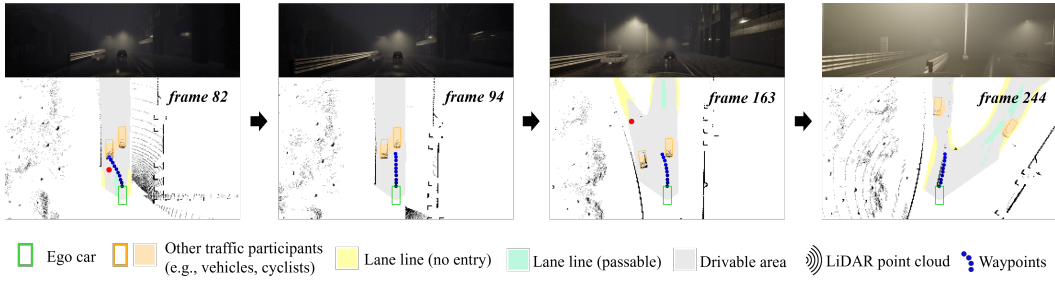


403 Figure 4: On the same scene as in Fig. 3, overtaking maneuver performed by **BridgeDrive<sup>geo</sup>**. The  
404 ego vehicle adapts its planning to overtake a sequence of parked cars. For video demon-  
405 stration, please refer to supplementary materials.

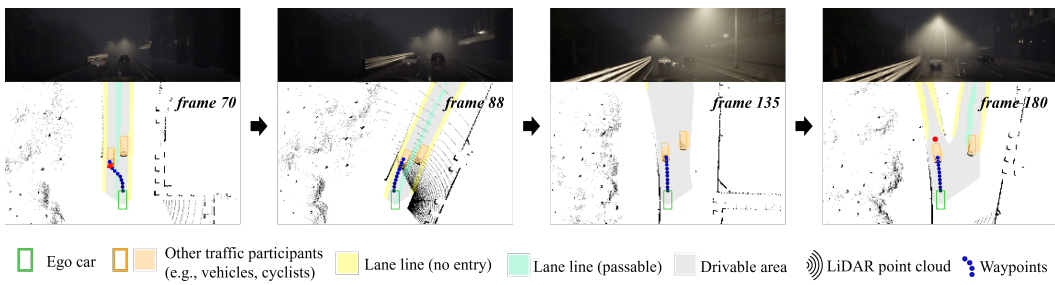
406  
407 bridge policy with anchor guidance differs from other diffusion planners. [Further ablation study](#)  
408 [results on the influence of anchors and classifiers are provided in Appendix D](#).

409 **Effectiveness of the representation of geometric path waypoints.** To account for the influence of  
410 different representations of the trajectory, namely the temporal speed waypoints vs. geometric path  
411 waypoints, we implement these two configurations for each version of diffusion models, denoted as  
412 *temp* and *geo*, respectively. It should be noted that, for DiffusionDrive<sup>geo</sup>, all modules remain iden-  
413 tical to those of our method except for the diffusion part to ensure a fair comparison. The results are  
414 compared in Table 2. It can be seen that the representation of geometric path waypoints outperforms  
415 their temporal counterpart, with an improvement of +5.46%, +9.09%, +12.37% in the success rate  
416 for DiffusionDrive, Full Diffusion, BridgeDrive, respectively. We argue the main reasons for this  
417 are as follows. 1) Temporal waypoints encode speed control information in the spacing between  
418 subsequent waypoints. Such an encoding is ambiguous and difficult to generalize. For example, for  
419 overtaking maneuvers with different speeds, geometric waypoints only require a model to learn the  
420 similar geometric pattern of driving path plus a varying speed scalar. In comparison, the general-  
421 ization of temporal waypoints require a model to stretch spacing between waypoints to account for  
422 different speeds. 2) Geometric waypoints are more compliant with route topology and is therefore  
423 less likely to violate route lane constrain; similar arguments are also provided in (Jaeger et al., 2023).

424 **The advantage of BridgeDrive model.** As illustrated in Table 2, benefiting from the multi-modality  
425 of diffusion models, both Full Diffusion<sup>geo</sup> and BridgeDrive<sup>geo</sup> outperform DiffusionDrive<sup>geo</sup> by  
426 a large margin. In addition, compared with full diffusion, BridgeDrive further leverages anchor  
427 information to guide its diffusion process. This is of particular importance when facing ambiguous  
428 situations. An example is visualized in Fig. 5 and Fig. 6. In this case, the target point for lane  
429 change is given in a short distance ahead of the ego vehicle. Due to inherent inertial of the ego car,  
430 it is unlikely for full diffusion to change lane. Therefore, the ego car kept traveling in a straight path  
431 and missed the target point; subsequently, the ego car was unable to make a sharp turn to the left  
432 lane and hit the road barrier. In comparison, BridgeDrive, under the strong guidance of the anchor,  
433 was able to strictly follow the target point and entered the correct lane at the road fork.



442 Figure 5: **Full Diffusion model** in a consecutive four frames of a sample Bench2Drive scene. It  
443 **failed** to adhere to the target time window for lane-changing maneuvers, which consequently led to  
444 a collision with the road barrier. For video demonstration, please refer to supplementary materials.



453 Figure 6: **BridgeDrive** on the same scene as in Fig. 5. The BridgeDrive model **achieved** timely  
454 lane changing due to anchor guidance and successfully navigated through the road fork. For video  
455 demonstration, please refer to supplementary materials.

456 Table 2: Ablation study for the effects of temporal and geometric path waypoints for DiffusionDrive,  
457 full diffusion, and BridgeDrive. All methods use identical modules except for the diffusion part. Our  
458 BridgeDrive<sup>geo</sup> achieves SOTA DS and SR, prioritizing safety over Comfortness.

Configuration	Principled	Anchor	DS	SR(%)	Efficiency	Comfortness
DiffusionDrive <sup>temp</sup>	✗	✓	77.68	52.72	248.18	24.56
DiffusionDrive <sup>geo</sup>	✗	✓	80.79	58.18	245.34	15.49
Full Diffusion <sup>temp</sup>	✓	✗	79.75	58.18	246.31	24.42
Full Diffusion <sup>geo</sup>	✓	✗	83.85	67.27	238.90	21.40
BridgeDrive <sup>temp</sup>	✓	✓	81.97	59.90	243.88	22.61
BridgeDrive <sup>geo</sup>	✓	✓	87.99 ± 0.67	74.99 ± 1.35	236.49 ± 2.32	20.98 ± 0.74

## 5 CONCLUSIONS AND FUTURE WORK

We presented BridgeDrive—an autonomous driving solution based on diffusion bridge policy. Our method provides a principled bridge diffusion framework incorporating anchor guidance and outperformed prior work by **7.72%** in success rate. Extensive experiments validated that BridgeDrive yielded significant performance improvements in closed-loop planning tasks.

**Limitations and future work.** (1) While some existing methods only relies on camera input (e.g., Renz et al. (2025)), BridgeDrive also requires lidar input. Future work is expected to investigate BridgeDrive’s capability in the absence of lidar. (2) Although the inference speed of BridgeDrive is suitable for real-time deployment, further acceleration can be achieved by distilling our model into a one-step model without sacrificing the generation quality (Xie et al., 2024). (3) Despite BridgeDrive’s extraordinary capacity to learn complex planning tasks, it still struggles to handle out-of-distribution scenarios, as illustrated in Appendix B.3. This limitation may be overcome by incorporating prior knowledge from VLA and post-training with reinforcement learning.

486 REFERENCES  
487

488 Jens Beißwenger. PDM-lite: A rule-based planner for Carla leaderboard 2.0. Technical report,  
489 University of Tübingen, 2024.

490 Holger Caesar, Varun Bankiti, Alex H. Lang, Sourabh Vora, Venice Erin Liong, Qiang Xu, Anush  
491 Krishnan, Yu Pan, Giancarlo Baldan, and Oscar Beijbom. nuScenes: A multimodal dataset for  
492 autonomous driving. *arXiv preprint arXiv:1903.11027*, 2019.

493 Yuning Chai, Benjamin Sapp, Mayank Bansal, and Dragomir Anguelov. MultiPath: Multiple proba-  
494 bility anchor trajectory hypotheses for behavior prediction. In *Proceedings of the Conference on*  
495 *Robot Learning*, volume 100 of *Proceedings of Machine Learning Research*, pp. 86–99. PMLR,  
496 2020.

497 Dian Chen and Philipp Krähenbühl. Learning from all vehicles. In *Proceedings of the IEEE/CVF*  
498 *Conference on Computer Vision and Pattern Recognition*, pp. 17222–17231, 2022.

499 Shaoyu Chen, Bo Jiang, Hao Gao, Bencheng Liao, Qing Xu, Qian Zhang, Chang Huang, Wenyu  
500 Liu, and Xinggang Wang. Vadv2: End-to-end vectorized autonomous driving via probabilistic  
501 planning. *arXiv preprint arXiv:2402.13243*, 2024.

502 Kashyap Chitta, Aditya Prakash, Bernhard Jaeger, Zehao Yu, Katrin Renz, and Andreas Geiger.  
503 TransFuser: Imitation with transformer-based sensor fusion for autonomous driving. *IEEE Trans-*  
504 *actions on Pattern Analysis and Machine Intelligence*, 2023.

505 Daniel Dauner, Marcel Hallgarten, Tianyu Li, Xinshuo Weng, Zhiyu Huang, Zetong Yang,  
506 Hongyang Li, Igor Gilitschenski, Boris Ivanovic, Marco Pavone, Andreas Geiger, and Kashyap  
507 Chitta. NAVSIM: Data-driven non-reactive autonomous vehicle simulation and benchmarking.  
508 In *Advances in Neural Information Processing Systems (NeurIPS)*, 2024.

509 Joseph L Doob and JI Doob. *Classical potential theory and its probabilistic counterpart*, volume  
510 262. Springer, 1984.

511 Alexey Dosovitskiy, German Ros, Felipe Codevilla, Antonio Lopez, and Vladlen Koltun. CARLA:  
512 An open urban driving simulator. In Sergey Levine, Vincent Vanhoucke, and Ken Goldberg  
513 (eds.), *Proceedings of the 1st Annual Conference on Robot Learning*, volume 78 of *Proceedings*  
514 *of Machine Learning Research*, pp. 1–16. PMLR, 2017.

515 Haoyu Fu, Diankun Zhang, Zongchuang Zhao, Jianfeng Cui, Dingkang Liang, Chong Zhang,  
516 Dingyuan Zhang, Hongwei Xie, Bing Wang, and Xiang Bai. ORION: A holistic end-to-end au-  
517 tonomous driving framework by vision-language instructed action generation. *arXiv:2503.19755*,  
518 2025.

519 K. Tan et al. H. Caesar, J. Kabzan. Nuplan: A closed-loop ml-based planning benchmark for au-  
520 tonomous vehicles. In *CVPR ADP3 workshop*, 2021.

521 Jonathan Ho and Tim Salimans. Classifier-free diffusion guidance. In *NeurIPS 2021 Workshop on*  
522 *Deep Generative Models and Downstream Applications*, 2021.

523 Jonathan Ho, Ajay Jain, and Pieter Abbeel. Denoising diffusion probabilistic models. *Advances in*  
524 *neural information processing systems*, 33:6840–6851, 2020.

525 Yihan Hu, Jiazhi Yang, Li Chen, Keyu Li, Chonghao Sima, Xizhou Zhu, Siqi Chai, Senyao Du, Tian-  
526 wei Lin, Wenhui Wang, Lewei Lu, Xiaosong Jia, Qiang Liu, Jifeng Dai, Yu Qiao, and Hongyang  
527 Li. Planning-oriented autonomous driving. In *Proceedings of the IEEE/CVF Conference on Com-*  
528 *puter Vision and Pattern Recognition (CVPR)*, pp. 17853–17862, 2023.

529 Bernhard Jaeger, Kashyap Chitta, and Andreas Geiger. Hidden biases of end-to-end driving models.  
530 In *Proc. of the IEEE International Conf. on Computer Vision (ICCV)*, 2023.

531 Xiaosong Jia, Zhenjie Yang, Qifeng Li, Zhiyuan Zhang, and Junchi Yan. Bench2Drive: Towards  
532 multi-ability benchmarking of closed-loop end-to-end autonomous driving. In *NeurIPS 2024*  
533 *Datasets and Benchmarks Track*, 2024.

540 Xiaosong Jia, Junqi You, Zhiyuan Zhang, and Junchi Yan. DriveTransformer: Unified transformer  
 541 for scalable end-to-end autonomous driving. In *International Conference on Learning Representations*, 2025.

543

544 Bo Jiang, Shaoyu Chen, Qing Xu, Bencheng Liao, Jiajie Chen, Helong Zhou, Qian Zhang, Wenyu  
 545 Liu, Chang Huang, and Xinggang Wang. VAD: Vectorized scene representation for efficient  
 546 autonomous driving. *ICCV*, 2023.

547

548 Xuefeng Jiang, Yuan Ma, Pengxiang Li, Leimeng Xu, Xin Wen, Kun Zhan, Zhongpu Xia, Peng  
 549 Jia, XianPeng Lang, and Sheng Sun. TransDiffuser: End-to-end trajectory generation with decor-  
 550 related multi-modal representation for autonomous driving. *arXiv preprint arXiv:2505.09315*,  
 551 2025.

551

552 Tero Karras, Miika Aittala, Timo Aila, and Samuli Laine. Elucidating the design space of diffusion-  
 553 based generative models. *Advances in neural information processing systems*, 35:26565–26577,  
 554 2022.

555

556 Diederik Kingma, Tim Salimans, Ben Poole, and Jonathan Ho. Variational diffusion models. *Ad-  
 557 vances in neural information processing systems*, 34:21696–21707, 2021.

557

558 Qifeng Li, Xiaosong Jia, Shaobo Wang, and Junchi Yan. Think2Drive: Efficient reinforcement  
 559 learning by thinking in latent world model for quasi-realistic autonomous driving (in CARLA-  
 560 v2). In *Proceedings of the European Conference on Computer Vision (ECCV)*, 2024a.

561

562 Zhenxin Li, Kailin Li, Shihao Wang, Shiyi Lan, Zhiding Yu, Yishen Ji, Zhiqi Li, Ziyue Zhu, Jan  
 563 Kautz, Zuxuan Wu, Yu-Gang Jiang, and Jose M. Alvarez. Hydra-MDP: End-to-end multimodal  
 564 planning with multi-target hydra-distillation. *arXiv preprint arXiv:2406.06978*, 2024b.

564

565 Bencheng Liao, Shaoyu Chen, Haoran Yin, Bo Jiang, Cheng Wang, Sixu Yan, Xinbang Zhang,  
 566 Xiangyu Li, Ying Zhang, Qian Zhang, et al. DiffusionDrive: Truncated diffusion model for  
 567 end-to-end autonomous driving. In *Proceedings of the Computer Vision and Pattern Recognition  
 Conference*, pp. 12037–12047, 2025.

568

569 Ilya Loshchilov and Frank Hutter. Decoupled weight decay regularization. *arXiv preprint  
 570 arXiv:1711.05101*, 2017a.

571

572 Ilya Loshchilov and Frank Hutter. SGDR: Stochastic gradient descent with warm restarts. In *Inter-  
 573 national Conference on Learning Representations*, 2017b.

574

575 Cheng Lu, Yuhao Zhou, Fan Bao, Jianfei Chen, Chongxuan Li, and Jun Zhu. DPM-solver: A fast  
 576 ode solver for diffusion probabilistic model sampling in around 10 steps. *Advances in neural  
 577 information processing systems*, 35:5775–5787, 2022.

577

578 Katrin Renz, Long Chen, Elahe Arani, and Oleg Sinavski. Simlingo: Vision-only closed-loop au-  
 579 tonomous driving with language-action alignment. In *Conference on Computer Vision and Pattern  
 580 Recognition (CVPR)*, 2025.

581

582 Abbas Sadat, Sergio Casas, Mengye Ren, Xinyu Wu, Pranaab Dhawan, and Raquel Urtasun. Per-  
 583 ceive, predict, and plan: Safe motion planning through interpretable semantic representations. In  
 584 *Proceedings of the European Conference on Computer Vision (ECCV)*, 2020.

585

586 Chonghao Sima, Katrin Renz, Kashyap Chitta, Li Chen, Hanxue Zhang, Chengen Xie, Jens  
 587 Beßwenger, Ping Luo, Andreas Geiger, and Hongyang Li. DriveLM: Driving with graph vi-  
 588 sual question answering. In *European Conference on Computer Vision (ECCV)*, pp. 256–274.  
 Springer, 2025.

589

590 Jascha Sohl-Dickstein, Eric Weiss, Niru Maheswaranathan, and Surya Ganguli. Deep unsupervised  
 591 learning using nonequilibrium thermodynamics. In *International conference on machine learn-  
 592 ing*, pp. 2256–2265. PMLR, 2015.

593

Jiaming Song, Chenlin Meng, and Stefano Ermon. Denoising diffusion implicit models. In *Interna-  
 594 tional Conference on Learning Representations*, 2021a.

594 Yang Song, Jascha Sohl-Dickstein, Diederik P Kingma, Abhishek Kumar, Stefano Ermon, and Ben  
 595 Poole. Score-based generative modeling through stochastic differential equations. In *International*  
 596 *Conference on Learning Representations*, 2021b.

597

598 Pascal Vincent. A connection between score matching and denoising autoencoders. *Neural computation*,  
 599 23(7):1661–1674, 2011.

600 Penghao Wu, Xiaosong Jia, Li Chen, Junchi Yan, Hongyang Li, and Yu Qiao. Trajectory-guided  
 601 control prediction for end-to-end autonomous driving: A simple yet strong baseline. In *Advances*  
 602 *in Neural Information Processing Systems*, 2022.

603

604 Sirui Xie, Zhisheng Xiao, Diederik Kingma, Tingbo Hou, Ying Nian Wu, Kevin P Murphy, Tim  
 605 Salimans, Ben Poole, and Ruiqi Gao. EM distillation for one-step diffusion models. *Advances in*  
 606 *Neural Information Processing Systems*, 37:45073–45104, 2024.

607

608 Zebin Xing, Xingyu Zhang, Yang Hu, Bo Jiang, Tong He, Qian Zhang, Xiaoxiao Long, and Wei  
 609 Yin. GoalFlow: Goal-driven flow matching for multimodal trajectories generation in end-to-end  
 610 autonomous driving. *arXiv preprint arXiv:2503.05689*, 2025.

611

612 Zhenhua Xu, Yan Bai, Yujia Zhang, Zhuoling Li, Fei Xia, Kwan-Yee K. Wong, Jianqiang Wang, and  
 613 Hengshuang Zhao. DriveGPT4-V2: Harnessing large language model capabilities for enhanced  
 614 closed-loop autonomous driving. In *Proceedings of the IEEE/CVF Conference on Computer*  
 615 *Vision and Pattern Recognition (CVPR)*, 2025.

616

617 Brian Yang, Huangyuan Su, Nikolaos Gkanatsios, Tsung-Wei Ke, Ayush Jain, Jeff Schneider, and  
 618 Katerina Fragkiadaki. Diffusion-ES: Gradient-free planning with diffusion for autonomous driv-  
 619 ing and zero-shot instruction following. *arXiv preprint arXiv:2402.06559*, 2024.

620

621 Xuemeng Yang, Licheng Wen, Tiantian Wei, Yukai Ma, Jianbiao Mei, Xin Li, Wenjie Lei, Daocheng  
 622 Fu, Pinlong Cai, Min Dou, Liang He, Yong Liu, Botian Shi, and Yu Qiao. Drivearena: A closed-  
 623 loop generative simulation platform for autonomous driving. In *Proceedings of the IEEE/CVF*  
 624 *International Conference on Computer Vision (ICCV)*, pp. 26933–26943, October 2025.

625

626 Zhejun Zhang, Alexander Liniger, Dengxin Dai, Fisher Yu, and Luc Van Gool. End-to-end urban  
 627 driving by imitating a reinforcement learning coach. In *Proceedings of the IEEE/CVF Interna-*  
 628 *tional Conference on Computer Vision (ICCV)*, 2021.

629

630 Kaiwen Zheng, Guande He, Jianfei Chen, Fan Bao, and Jun Zhu. Diffusion bridge implicit models.  
 631 In *The Thirteenth International Conference on Learning Representations*, 2025a.

632

633 Yinan Zheng, Ruiming Liang, Kexin ZHENG, Jinliang Zheng, Liyuan Mao, Jianxiong Li, Wei-  
 634 hao Gu, Rui Ai, Shengbo Eben Li, Xianyuan Zhan, and Jingjing Liu. Diffusion-based planning  
 635 for autonomous driving with flexible guidance. In *The Thirteenth International Conference on*  
 636 *Learning Representations*, 2025b.

637

638 Linqi Zhou, Aaron Lou, Samar Khanna, and Stefano Ermon. Denoising diffusion bridge models. In  
 639 *The Twelfth International Conference on Learning Representations*, 2024.

640

641 Julian Zimmerlin, Jens Beißwenger, Bernhard Jaeger, Andreas Geiger, and Kashyap Chitta. Hidden  
 642 biases of end-to-end driving datasets. *arXiv preprint arXiv:2412.09602*, 2024.

643

644

645

646

647

648  
649  
650  
651 Table 3: Comprehensive comparison between BridgeDrive and Baselines. BridgeDrive prioritizes  
652 safety over Comfortness.  
653  
654

Method	Expert	Key technique	DS	SR(%)	Effi.	Comfort.
DiffusionDrive <sup>temp</sup>	PDM-Lite	Diffusion	77.68	52.72	248.18	24.56
TCP-traj*	Think2Drive	CNN, MLP, GRU	59.90	30.00	76.54	18.08
UniAD-Base	Think2Drive	Transformer	45.81	16.36	129.21	43.58
VAD	Think2Drive	Transformer	42.35	15.00	157.94	46.01
DriveTransformer	Think2Drive	Transformer	63.46	35.01	100.64	20.78
ORION	Think2Drive	VLA+VAE	77.74	54.62	151.48	17.38
ORION diffusion	Think2Drive	VLA+Diffusion	71.97	46.54	NA	NA
SimLingo	PDM-Lite	VLA	85.07	67.27	259.23	33.67
TransFuser++	PDM-Lite	Transformer	84.21	67.27	NA	NA
BridgeDrive (ours)	PDM-Lite	Diffusion	87.99 (+2.72)	74.99 (+7.72)	236.49	20.98

## 666 A RELATED WORK 667

668  
669 **End-to-end autonomous driving.** Traditional motion planning pipelines often decompose the task  
670 into separate stages—perception, prediction, and planning—which inevitably introduce latency and  
671 information degradation across modules (Sadat et al., 2020). To overcome these limitations, recent  
672 studies have shifted toward planning-centric, end-to-end autonomous driving frameworks. End-to-  
673 end autonomous driving aims to map raw sensory inputs directly to trajectory predictions or control  
674 commands, enabling holistic system optimization that mitigates error propagation across modules  
675 (Wu et al., 2022; Zhang et al., 2021). UniAD (Hu et al., 2023) shows the feasibility of end-to-  
676 end autonomous driving by unifying multiple perception tasks to benefit planning. Building on  
677 this, VAD (Jiang et al., 2023) introduces compact vectorized scene representations to boost effi-  
678 ciency. VADv2 (Chen et al., 2024) proposes a probabilistic planning framework that models the  
679 distribution over possible actions and samples one for vehicle control. SimLingo (Renz et al., 2025)  
680 and GPTDriverV2 (Xu et al., 2025) incorporate vision-language understanding and language-action  
681 alignment, aiming to enhance closed-loop driving performance.

682 **Deterministic planners.** Some end-to-end autonomous driving planners relies on models such as  
683 multilayer perceptrons (MLPs) or variational autoencoders (VAEs). Transfuser (Chitta et al., 2023)  
684 and its extension Transfuser++ (Jaeger et al., 2023) exemplify this line of work by fusing multi-  
685 modal sensor inputs—such as camera images and LiDAR point clouds—through transformer-based  
686 encoders and decoding them into trajectory outputs via compact MLP heads. These models highlight  
687 the importance of effective sensor fusion in improving closed-loop driving performance. ORION (Fu  
688 et al., 2025) adopts a VAE-based latent planning architecture, which enables the model to capture  
689 multi-modal trajectory distributions while maintaining computational efficiency. These methods  
690 demonstrate how MLP and VAE-style architectures can serve as efficient baselines for end-to-end  
691 planning, though they often face limitations in modeling the full multi-modality of human driving  
692 behaviors compared to generative paradigms such as diffusion or flow-based models.

693 **Diffusion-based planners.** Diffusion policies provide a generative paradigm which can model  
694 the multi-modal nature of human driving behaviors with enhanced guidance control. Diffusion-ES  
695 (Yang et al., 2024) exhibits zero-shot instruction-following ability in planning. Diffusion-Planner  
696 (Zheng et al., 2025b) uses joint prediction modeling to achieve safe and adaptive planning. GoalFlow  
697 (Xing et al., 2025) leverages flow matching to produce diverse goal-conditioned trajectories and  
698 further uses a trajectory scorer to efficiently select trajectory using the goal point as a reference.  
699 DiffusionDrive (Liao et al., 2025) points out the issue of mode collapse, wherein the generated  
700 trajectories lack diversity, as different random noise inputs tend to converge to similar trajectories  
701 during the denoising process, proposing truncated diffusion policy that begins the denoising process  
702 from an anchored gaussian distribution instead of a standard Gaussian distribution to avoid mode  
703 collapse. TransDiffuser (Jiang et al., 2025) emphasizes another underlying bottleneck that leads to  
704 mode collapse in generated trajectories: The under-utilization of the encoded multi-modal condi-

702 Table 4: Multi-Ability evaluation results. BridgeDrive outperforms all baselines in all categories  
 703 except for Give Way.

705 706 707 708 709 710 711 712 713 714 715 716 717 718	Ability (%)					
	Merg.	Overtak.	Emer. Brake	Give Way	Traf. Sign	Mean
DiffusionDrive <sup>temp</sup>	50.63	26.67	68.33	50.00	76.32	54.38
TCP-traj*	8.89	24.29	51.67	40.00	46.28	34.22
UniAD-Base	14.10	17.78	21.67	10.00	14.21	15.55
VAD	8.11	24.44	18.64	20.00	19.15	18.07
DriveTransformer	17.57	35.00	48.36	40.00	52.10	38.60
ORION	25.00	71.11	78.33	30.00	69.15	54.72
SimLingo	54.01	57.04	88.33	53.33	82.45	67.03
TransFuser++	58.75	57.77	83.33	40.00	82.11	64.39
BridgeDrive (ours)	<b>69.92</b> (+10.87)	<b>66.67</b> (-4.44)	<b>90.00</b> (+1.67)	<b>50.00</b> (-3.33)	<b>89.47</b> (+7.02)	<b>73.15</b> (+6.12)

719  
 720 Table 5: Inference wall-clock time comparison. The full diffusion model is approximately half the  
 721 size of BridgeDrive, as it does not have cross-attention modules for anchors. BridgeDrive achieves  
 722 reasonable inference speed even without any additional optimization, indicating its suitability for  
 723 real-time deployment.

724 725	Configuration	Inference speed per frame	#diffusion timesteps
726	DiffusionDrive <sup>temp</sup>	0.05 sec	2
727	DiffusionDrive <sup>geo</sup>	0.05 sec	2
728	Full Diffusion <sup>temp</sup>	0.05 sec	100
729	Full Diffusion <sup>geo</sup>	0.05 sec	100
730	BridgeDrive <sup>temp</sup>	0.10 sec	20
731	BridgeDrive <sup>geo</sup>	0.10 sec	20

734  
 735 tional information. Therefore, it implements multi-modal representation decorrelation optimization  
 736 mechanism during the denoising process, which aims to better exploit the multi-modal representa-  
 737 tion space to guide more diverse feasible planning trajectories from the continuous action space.

## 739 B ADDITIONAL RESULTS, VISUALIZATION AND LIMITATION

### 741 B.1 COMPARISON WITH EXISTING WORKS

743 A comprehensive evaluation on Bench2Drive metrics is provided in Tables 3 and 4. Our  
 744 method shows SOTA performance on both Driving Score (DS) and Success Rate (SR). **Moreover,**  
 745 **BridgeDrive exhibits outstanding multi-ability capability, especially in Merging (+10.87), and Traf-**  
 746 **fic Sign (+7.02), resulting in overall improvement by +6.12 than SOTA.** However, BridgeDrive  
 747 demonstrates suboptimal performance in the Comfortness and Give Way metrics, suggesting a ten-  
 748 dency toward frequent or poorly timed braking. This outcome may imply that our model prioritizes  
 749 safety considerations, potentially at the expense of passenger comfort. This limitation should be  
 750 addressed in the future work.

### 751 B.2 INFERENCE SPEED

753 Inference wall-clock time comparison is detailed in Table 5. Note that the full diffusion model is  
 754 slightly faster than BridgeDrive since it is approximately half the size of BridgeDrive. This is be-  
 755 cause full diffusion does not use anchors and thus omit all anchor-related cross-attention modules.  
 BridgeDrive achieves reasonable inference speed even without any additional optimization, indicat-

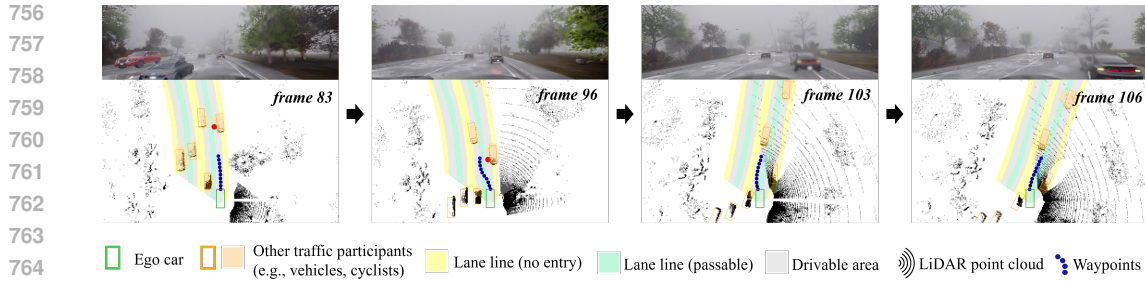


Figure 7: BridgeDrive cannot handle imperfect timing of lane-changing, which resulted from cumulative errors. This situation is outside of the training data distribution.

ing its suitability for real-time deployment. It should be noted that in both DiffusionDrive and our BridgeDrive model, the primary computational cost stems from the perception and cross-attention modules. The diffusion process itself is applied only to a small trajectory matrix ( $8 \times 2$  or  $11 \times 2$ ), contributing a minor portion of the total cost. Consequently, the overall computation time does not increase proportionally with the number of diffusion steps.

### B.3 CASE STUDY FOR AN OUT-OF-DISTRIBUTION SCENARIO

Despite the extraordinary modeling capacity of BridgeDrive, it cannot generalize to out-of-distribution scenarios, which is very common in closed-loop evaluation. For instance, the overtaking maneuver shall be aborted if oncoming vehicles are present in the adjacent lane. However, there are almost no such data in the training set. The reason is that training data are collected by a rule-based expert with privileged information (i.e., the expert has direct access to the ground truth of other traffic participants' location and dynamics). This expert has long-term planning capability and will only perform an overtaking maneuver when there is sufficient longitudinal space in adjacent lanes. Such an ideal timing is not always feasible in closed-loop evaluation due to cumulative difference between predicted and ground-truth speed. An example of imperfect timing for lane changing is provided in Fig. 7. This limitation may be overcome by integrating scene understanding prior knowledge from VLA into BridgeDrive or posting-training with reinforcement learning, which is left for future work.

### B.4 EXPERIMENTS ON ADDITIONAL BENCHMARKS

We conducted additional evaluations of our method on the NAVSIM dataset, adhering to the metrics established in DiffusionDrive (Liao et al., 2025). These metrics are summarized by the PDM score (PDMS), a weighted composite of no at-fault collisions (NC), drivable area compliance (DAC), time-to-collision (TTC), comfort (Comf.), and ego progress (EP). As shown in Table 6, our proposed BridgeDrive achieves competitive performance on NAVSIM. We posit that this performance is notable, as NAVSIM is a mature dataset, where existing state-of-the-art models have already saturated its performance potential (NAVSIM is an open-loop dataset with non-reactive agents that does not capture real-world driving behavior, as they artificially reset the agent to the ground-truth state at every step, preventing error accumulation).

For this reason, our paper primarily targets the more realistic closed-loop setting (i.e., Bench2Drive), as emphasized in the paper title. The closed-loop setting is more challenging and better reflects a policy's real-world planning capability, since the ego vehicle's decisions influence both its own future states and those of surrounding agents. This interaction creates a feedback loop that can amplify small prediction errors over time, as discussed in Section 2.1. We also highlight that evaluating in closed-loop settings has become an emerging trend in the autonomous driving community (Chitta et al., 2023; Zheng et al., 2025b; H. Caesar, 2021; Yang et al., 2025; Jia et al., 2024), driving more realistic assessments that better reflect actual technological progress. Our experimental results demonstrated that our BridgeDrive method outperformed previous state-of-the-art methods in this challenging setting.

810  
811  
812 **Table 6: Performance comparison on planning-oriented NAVSIM navtest split.**  
813  
814  
815  
816  
817  
818  
819

	NC	DAC	TTC	Comf.	EP	PDMS
VADv2-V <sub>8192</sub> (Chen et al., 2024)	97.2	89.1	91.6	100	76.0	80.9
Hydra-MDP-V <sub>8192</sub> -W-EP (Li et al., 2024b)	98.3	96	94.6	100	78.7	86.5
DiffusionDrive (reported in Liao et al. (2025))	98.2	96.2	94.7	100	82.2	88.1
DiffusionDrive (reproduced with a different seed)	98.2	95.9	94.3	100	81.9	87.6
BridgeDrive (ours)	98.2	96.1	94.5	100	82.3	88.0

820  
821 **B.5 THE SUPERIORITY OF GEOMETRIC WAYPOINTS REMAINS UNDEREXPLORED**  
822823 We briefly summarizes key experimental findings regarding temporal and geometric waypoints in  
824 autonomous driving models:  
825

- 826 1. A prominent line of research has achieved SOTA performance primarily through the use  
827 of temporal waypoints (Liao et al., 2025; Zheng et al., 2025b; Chitta et al., 2023; Chen &  
828 Krähenbühl, 2022; Wu et al., 2022).
- 829 2. TransFuser++ (Jaeger et al., 2023) identified ambiguities inherent in temporal waypoints.  
830 To address this, the authors implemented a path predictor (analogous to our geometric waypoints)  
831 and a speed predictor. The speed is predicted via an MLP head using classification,  
832 which also outputs an associated uncertainty. Their experiments demonstrated that inter-  
833 polating between target speeds, weighted by this uncertainty, effectively reduces collision  
834 rates.
- 835 3. SimLingo (Renz et al., 2025) trained a Vision-Language Model (VLM) to predict both tem-  
836 poral and geometric waypoints (termed “temporal speed waypoints” and “geometric path  
837 waypoints,” respectively). They found that using only temporal waypoints resulted in poor  
838 steering performance, whereas incorporating geometric waypoints significantly improved  
839 vehicle control. In their framework, the control commands are derived from both repre-  
840 sentations: target speed is computed from temporal waypoints, while the steering angle is  
841 determined by geometric waypoints.
- 842 4. DriveGPT4-V2 (Xu et al., 2025) does not directly output waypoints for control. Instead, it  
843 predicts a target speed and steering angle directly, using temporal and geometric waypoints  
844 (referred to as “waypoints” and “route points”) solely as supervisory signals during train-  
845 ing. Their ablation study concluded that predicting the final control commands (speed and  
846 angle) is more effective than predicting intermediate waypoints.

847 These findings suggest that optimal control performance may not be achieved by relying exclusively  
848 on either temporal or geometric waypoints. Instead, superior performance likely arises from the  
849 interplay between these two representations and their derived control variables. The field has not yet  
850 reached a definitive conclusion on this matter.851 A comprehensive understanding of the fundamental roles of temporal and geometric waypoints  
852 would require an extensive experimental evaluation of various SOTA algorithms across multiple  
853 mainstream benchmarks, which is left for future work. Therefore, in our experiments, we adopt  
854 the conventional practice established by TransFuser++ (Jaeger et al., 2023), as our model architec-  
855 ture most closely resembles theirs. Consequently, the experiments presented in this paper primarily  
856 demonstrate the superiority of geometric waypoints within the Bench2Drive benchmark.  
857858 **C EXPERIMENT DETAILS**  
859860 **C.1 DATASETS FILTERING AND AUGMENTATION**  
861862 Zimmerlin et al. (2024) proposed a data filtering method to reduce redundancy in training datasets.  
863 The method involves keeping frames where significant changes occur compared to the previous  
864 frame. Specifically, a frame is retained if either of the following conditions is met.

864 Table 7: Comparison among the major modules in the model architectures of DiffusionDrive,  
 865 DiffusionDrive<sup>temp</sup>, DiffusionDrive<sup>geo</sup>, and BridgeDrive.  
 866

Module	DiffusionDrive	DiffusionDrive <sup>temp</sup>	DiffusionDrive <sup>geo</sup>	BridgeDrive
Perception	Transfuser	Transfuser++	Transfuser++	Transfuser++
Classifier	Transfuser	Transfuser++	Transfuser++	BridgeDrive
Denoiser	DiffusionDrive	DiffusionDrive	DiffusionDrive	BridgeDrive
Output	Temporal waypoints	Temporal waypoints	Geometric waypoints	Geometric waypoints

874

- 875 • The target speed changes by more than 0.1 m/s.
- 876 • The angle to any predicted geometric path waypoints changes by more than 0.5°.

877

878 From the remaining frames, 14% are randomly selected and kept. This strategy results in a 50%  
 879 reduction in the dataset size.

880 Additionally, the authors adjust the expert’s driving style by modifying behaviors, such as the timing  
 881 of braking when approaching pedestrians. This adjustment ensures the expert’s actions are more  
 882 interpretable and provide clearer learning signals for the model. Furthermore, the paper removes  
 883 class weights for target speed values, particularly for over-represented classes like braking, to avoid  
 884 biasing the model towards more frequent behaviors. This ensures the model learns from frames  
 885 critical for driving tasks, rather than focusing on frequent but less important ones.

## 887 C.2 ADAPTATION OF DIFFUIONDRIVE TO BENCH2DRIVE BENCHMARK

889 We denote adapted versions of DiffusionDrive as DiffusionDrive<sup>temp</sup> and DiffusionDrive<sup>geo</sup>. We  
 890 explain our adaption from four aspects.

891 **Perception module.** The original DiffusionDrive was built on the backbone of Transfuser (Chitta  
 892 et al., 2023), whereas our BridgeDrive is based on Transfuser++ (Jaeger et al., 2023). To ensure  
 893 a competitive baseline for fair comparison, for the adaptation of DiffusionDrive, we use the per-  
 894 ception module from Transfuser++, which is proven to achieve SOTA on Bench2Drive benchmark  
 895 (Zimmerlin et al., 2024).

896 **Denoiser.** We keep the model architecture of the denoiser identical to its original design as it is  
 897 unique to each model under comparison.

899 **Classifier.** The classifier in DiffusionDrive consists of cross-attention modules to process the per-  
 900 ception features. We keep its architecture in line with the perception module.

901 **Output.** The output trajectory representation of DiffusionDrive<sup>temp</sup> is temporal waypoints, which  
 902 is kept the same as DiffusionDrive. The analysis of the impact of output representation is provided  
 903 in Section 4.3, where DiffusionDrive<sup>temp</sup>’s geometric waypoints counterpart DiffusionDrive<sup>geo</sup> is  
 904 implemented and evaluated.

905 An overview comparing the architectures of the major modules across DiffusionDrive,  
 906 DiffusionDrive<sup>temp</sup>, and BridgeDrive is provided in Table 7. The rest of the implementation and  
 907 training details of DiffusionDrive<sup>temp</sup> are kept the same as BridgeDrive for a fair comparison.

## 909 C.3 IMPLEMENTATION AND TRAINING DETAILS

911 As mentioned in Section 3.4, our model consists of three modules. For perception module, we keep  
 912 the original design as described in (Jaeger et al., 2023) and (Zimmerlin et al., 2024). Once the  
 913 perception module is pre-trained, it is frozen during the training phase of the denoiser and classifier  
 914 modules. The joint loss for the denoiser and classifier is defined as:

$$915 L_{\text{overall}} = w_{\text{diffusion}} L_{\text{diffusion}} + w_{\text{classification}} L_{\text{classification}}, \quad (11)$$

917 where  $L_{\text{diffusion}}$  is as defined in Eq. (9) and  $L_{\text{classification}}$  is the cross-entropy loss. By default, both  
 $w_{\text{diffusion}}$  and  $w_{\text{classification}}$  are set to 1. We optimize them using AdamW (Loshchilov & Hutter, 2017a)

918 **Table 8: Influence of anchor classification accuracy on the performance of BridgeDrive.**  
919

---

	Anchor-selected	Best	2nd best	3rd best	4th best
Success rate (%)	74.99	69.09	61.36	57.72	
Driving score	87.99	85.31	80.76	77.53	

---

920  
921  
922  
923  
924  
925  
926  
927 with a cosine annealing learning schedule (Loshchilov & Hutter, 2017b). The learning rate is set as  
928  $lr_0 = 3 \times 10^{-4}$ ,  $T_0 = 10$ ,  $T_{mult} = 2$ . In line with DiffusionDrive, we use  $N_{\text{anchor}} = 20$  anchors in  
929 BridgeDrive. Our models are trained for 10 epochs on a single H20 GPU, which takes around 10  
930 hours.

931 For diffusion schedule, we employ the variance preserving (VP) schedule from Karras et al. (2022).  
932 Specifically, we first define  $s(t) = 1/\sqrt{e^{\beta_d t^2/2 + \beta_{min} t}}$  and  $\sigma(t) = \sqrt{e^{\beta_d t^2/2 + \beta_{min} t} - 1}$ . We then  
933 set the diffusion coefficients in the forward diffusion bridge SDE Eq. (5) to  $f(t) = \dot{s}(t)/s(t)$  and  
934  $g(t) = \sqrt{2s(t)^2\dot{\sigma}(t)\sigma(t)}$ . We choose  $\beta_d = 2.0$  and  $\beta_{min} = 0.1$  following Zheng et al. (2025a).  
935

## 936 D ADDITIONAL ABLATION STUDY

### 937 D.1 INFLUENCE OF ANCHOR CLASSIFICATION ACCURACY

938 To assess the impact of anchor selection, we generated trajectories using sub-optimal anchors (i.e.,  
939 the 2nd, 3rd, and 4th most likely from the classifier). The result is presented in Table 8. Our bridge  
940 diffusion model exhibited significant resilience, achieving  $> 60\%$  success rate with the 2nd and 3rd  
941 anchors. However, both success rate and driving score decreased as lower-probability anchors were  
942 chosen, which demonstrate the importance of anchor classification accuracy.  
943

### 944 D.2 INFLUENCE OF DIFFUSION BRIDGE MODULE AND ANCHOR PRIOR

945 We perform ablation study to quantify the contribution of diffusion bridge module and anchor, re-  
946 spectively.  
947

948 To isolate the contribution of the diffusion blocks, we construct a BridgeDrive model with only 1  
949 anchor. As shown in Table 9, without the prior information of the anchor, the BridgeDrive model  
950 achieves a performance comparable to that of the full diffusion model in Table 2.  
951

952 To isolate the contribution of the diffusion blocks, we conducted an ablation where we used only  
953 the anchor selector (without any diffusion refinement) on the Bench2Drive benchmark. As shown in  
954 Table 9, the anchor-only model fails to achieve competent performance, even with a very large num-  
955 ber of anchors. This provides compelling evidence that diffusion blocks are essential for generating  
956 high-quality trajectories and are not merely minor enhancement.  
957

958 In addition, we constructed a regression model by removing the time-embedding component from  
959 our denoiser model while keeping the rest of the architecture unchanged. Table 9 shows that the  
960 anchor regression model performs consistently worse than our BridgeDrive model. This supports  
961 our claim that the iterative, probabilistic refinement provided by the diffusion bridge process in  
962 BridgeDrive is essential for achieving higher performance.  
963

### 964 D.3 INFLUENCE OF THE NUMBER OF ANCHORS

965 The impact of the number of anchors, which directly influences anchor diversity, was evaluated  
966 through an ablation study. The results in Table 9 indicate that BridgeDrive’s success rate initially  
967 rises with the number of anchors, peaking at 60 and affirming the positive role of diversity. A sub-  
968 sequent decline in performance suggests that a larger anchor set compromises classification accuracy.  
969 Consequently, the model’s optimal performance is achieved at an equilibrium between anchor diver-  
970 sity and classification precision.  
971

972  
 973  
 974  
 975  
 976  
 977  
 978  
 979  
 980  
 981  
 982  
 983  
 984  
 985  
 986  
 987  
 988  
 989  
 990  
 991

992 **Table 9: Influence of the number of anchors on the performance of BridgeDrive and anchor-based**  
 993 **models.**

Number of anchors	$k=1$	$k=20$	$k=40$	$k=60$	$k=80$	$k=200$	$k=500$	$k=1000$
<b>Success rate (%)</b>								
BridgeDrive	67.27	72.27	73.18	74.99	72.72	-	-	-
Anchor classification	-	2.72	8.18	16.81	19.54	25.92	36.81	36.36
Anchor-based regression	-	68.18	72.72	70.91	70.91	-	-	-
<b>Driving score</b>								
BridgeDrive	84.88	87.02	87.24	87.99	87.27	-	-	-
Anchor classification	-	27.71	35.78	45.43	49.02	57.89	63.12	62.3
Anchor-based regression	-	86.73	87.09	86.91	86.77	-	-	-

1007  
 1008  
 1009  
 1010  
 1011  
 1012  
 1013  
 1014  
 1015  
 1016  
 1017  
 1018  
 1019  
 1020  
 1021  
 1022  
 1023  
 1024  
 1025